Polyvinyl fluoride: Predicting polarization in a complex soft matter system

Polyvinyl fluoride: Predicting polarization in a complex soft matter system

Carl M. Frostenson [1], Pär A. T. Olsson [2,3] and Per Hyldgaard [1,*]

[1]*Department of Microtechnology and Nanoscience-MC2, Chalmers University of Technology, SE-412 96 Gothenburg, Sweden*
[2]*Materials Science and Applied Mathematics, Malmö University, SE-205 06 Malmö, Sweden*
[3]*Division of Mechanics, Materials and Component Design, Lund University, P. O. Box 118, SE-221 00 Lund, Sweden*

(Received 10 March 2024; revised 29 August 2024; accepted 18 October 2024; published 5 November 2024)

We use first-principle density functional theory (DFT) to predict properties for semicrystalline polyvinyl fluoride (PVF) and compare with polyvinylidiene fluoride. We note that the crystalline regions of PVF are complex in the sense that we lack a complete experimental characterization of the detailed atomic organization. We therefore turn to DFT to predict both the structure and associated materials properties, illustrating a possible work flow for complex soft-matter modeling. We rely on the nonempirical consistent-exchange van der Waals density functional version [K. Berland and P. Hyldgaard, Phys. Rev. B **89**, 035412 (2014)] and identify plausible ground-state and excited-state motifs. From there we predict the elastic response of the crystalline motifs, and an upper limit estimate of the PVF polarization at room temperature.

DOI: 10.1103/PhysRevMaterials.8.115603

I. INTRODUCTION

Fluorinated polymers have gained significant attention due to their unique structural, reactive, and dielectric properties [1–3]. Partially fluorinated polymers can have a considerable polarization response when in a semicrystalline form. This holds, for example, for the orthorhombic β phase of polyvinylidene fluoride (PVDF) [4–6]. There is also experimental evidence that orthorhombic polyvinyl fluoride (PVF) has a nonzero polar response [7,8]. PVF and PVDF are synthesized from vinyl fluoride ($CH_2 = CHF$) and vinylidene fluoride ($CH_2 = CF_2$) monomers, respectively. In comparison to polyethylene (PE), one substitutes either one (in PVF) or two (in PVDF) hydrogen atoms per repeat unit by fluorine atoms [9–12]. The well-explored PVDF [13] and less-explored PVF are not as chemically stable as fully fluorinated teflon, but may both work well for fuel cells (permeable membranes), capacitors (dielectric), and electromechanical sensing devices (hearing aids) [14–16]. They are expected to have an enhanced thermal [2] and mechanical [3] stability relative to PE, although we are not aware of any quantitative comparisons.

A key observation is that the asymmetric inclusion of fluorine atoms into a PE-type structure (forming PVF or β-PVDF), Fig. 1, can produce a considerable spontaneous polarizability P. This is well established for the metastable β-PVDF [4–6,13,17–19]. For fluorinated polymers like PVDF and PVF, the P value (of a perfectly annealed monocrystalline sample) depends on details of the atomic structure of the crystalline ground state (GS). In practice, the measured polarizability may also depend on the P values arising from metastable PVF/PVDF variants, provided they are close in per-unit-cell binding energy and structurally compatible to the GS structure. If the systems are also annealed to approach a thermal equilibrium, such motif inclusions would only survive if the interface energies can be ignored, i.e., if the inclusions have some size.

However, PVF is a soft-matter example of so-called complex matter, i.e., problems where materials-theory predictions are needed to sort out the nature of the system before we discuss the potential for a desired function, for example, as in Refs. [20,21]. Polymers exemplify the complex-matter challenge, as they typically exist at best in a semicrystalline state [22,23], where highly ordered crystalline regions are intertwined with disordered amorphous regions [22,24–26]. There is a consensus that PVF exhibits a relatively high crystallinity (40–60%) [7,8,27,28] and a planar zig-zag conformation [7,29], but the orthorhombic form and the tacticity are still under debate [8,27–32]. Meanwhile, conventional experimental investigation and exploration of functionality in semicrystalline polymers is challenging. If there is a polarization, then one would need annealed and carefully prepared semicrystalline samples of PVF to use it. But even in semicrystalline forms, different subregions need not have a would-be polarization pointing in the same direction [27,29]. With that comes the complication of the amorphous regions. PVDF has a glass transition temperature, $T_g \approx -35^\circ$C, whereas PVF exhibits several transitions with the lower T_g occuring at -15 to $-20\,^\circ$C and an upper T_g in the 40–50 °C range [26]. Amorphous regions will, generally, link crystalline blocks, significantly altering the overall response, making the macrolevel sample exhibit rubber or glass-state behaviors [33–35]. In spite of successful synthesis, existing

*Contact author: hyldgaar@chalmers.se

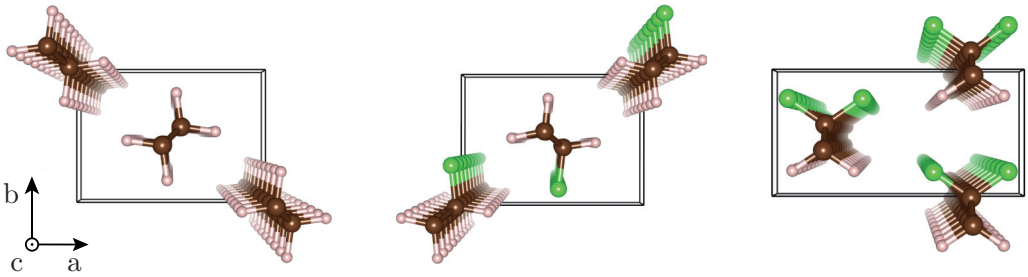

FIG. 1. Atomic structure, orthorhombic unit cells, and unit-cell vectors of the GS PE crystal (left), of the here-identified GS PVF motif (middle), and of the GS β-PVDF crystal (right). The GS PVF motif (GS β-PVDF) resembles GS PE, except that F atoms (green balls) replace one (two) of the H atoms (white balls) on every other carbon atom in the PE structure.

measurements alone do not suffice to assert whether PVF has any potential as a would-be flexible piezoelectrics.

Nonempirical (parameter-free) density functional theory (DFT) can check whether a material has potential for applications, i.e., help to tackle the complex matter challenge. DFT is the standard workhorse of *ab initio* material modeling at the atomic scale [36,37], because it offers a fast and efficient approach to predict properties, in principle, even before actual synthesis. This holds also for the weakly binding polymer systems thanks to the present-day (computationally efficient) inclusion of van der Waals (vdW) forces. For our soft-matter problems, we can either use a correction to semilocal DFT [38–49] or use the framework of the vdW density functional (vdW-DF) method [50–65] that keeps all interactions on the same electron-density foundation [66–70]. The use of such vdW-inclusive DFT allows us to not only resolve the PVF structure problem, but also predict polarization (and plastic [71–73]) properties. We can do that ahead of access to a fully controlled polymer-crystal sample.

Here we use the consistent-exchange vdW-DF-cx functional [68,74,75] (henceforth abbreviated "CX") to (1) determine the atomic and unit-cell structures as well as binding energies of a set of PVF crystalline conformers and (2) predict a set of properties for a plausible candidate for the PVF GS crystal, as well as for a limited set of excited-state (ES) conformers. We contrast the PVF predictions with those for the β-PVDF system [6,76]. CX is a strictly parameter-free version of the nonempirical vdW-DF method and, as such, a motivated choice for the present PVF focus, where we have insufficient data against which to optimize the choice of an empirical or semiempirical exchange-correlation (XC) functional [36,37]. The CX functional has proven to be an accurate tool for studying polymers in multiple crystalline phases, including response properties of nonpolar PE and polar PVDF [4–6,71,77].

In the present paper, we focus on communicating the wider potential of accurate, nonempirical (and transferable) theory in facing complex soft matter: We need such DFT to first aid in the structure-search stage and then to extract a set of materials-property predictions. We note that there is value in extending a structure-search stage by providing a set of materials predictions for a complex soft matter problem like PVF. Our point is that some of the materials-property predictions may be validated by observations while the rest of them are useful in lieu of yet-to-be-obtained experimental data. Accordingly, this paper predicts both the elastic and polarization response and will be supplemented by a forthcoming paper concerning plastic slip deformation [76], contrasting PE, PVF, and β-PVDF.

The set of panels in Fig. 1 compares our prediction for a plausible GS of PVF (middle panel) with the GS structure of the nonpolar PE (left panel) and of the polar β-PVDF (right panel). These semicrystalline systems are known to be orthorhombic. The PVF structure search, documented herein, identifies both the nonpolar GS structure and closely related metastable forms, of which several (for example, the orthorhombic motif ES2) have a high polarizability. At finite temperature, the system will comprise a mixture. Thus we predict that PVF can, in principle, be prepared to have a net room-temperature polarizability (under idealized conditions), but it is not as promising as a carefully prepared β-PVDF single-crystal sample [6].

The rest of the paper is organized as follows. In Sec. II we present the theoretical background and methods used in this work. In Sec. III we summarize computational details and outline the implementation of the theory. In Sec. IV we present and discuss our predictions. Finally, we summarize and conclude in Sec. V. Additionally, the paper contains an Appendix and Supplemental Material (SM) [78].

II. THEORY AND METHOD

The exact GS structure of PVF remains a topic of debate in the literature [29]. The interchain order in semicrystalline PVF is set by the competition of vdW attraction, Pauli repulsion, and (interchain) electrostatic interactions, a fact that puts demands on functional transferability [75]. Advanced approaches for molecule-crystal searches—sometimes combined with DFT predictions of atomic and unit-cell relaxations—are available [79,80] and will be necessary for facing general complex soft matter challenges (for example, for polymers with cross links). However, the stability, shape, and simplicity of the PE crystal and therefore of the (modified-PE) PVF and PVDF building blocks make our structure searches tractable. The systems can be modeled as formed by compact monomers of infinite length. The simplicity of monomers means that we can focus on exploring crystalline-motif candidates that differ in details of the interchain ordering and proceed essentially as previously illustrated for a prediction of plausible motifs for graphane stacking [81] or GS structure and magnetic ordering of ultrathin iron oxide films [82,83].

The PVF and PVDF chains are aligned in the c direction in all relevant unit cells (see Fig. 1). This holds both when setting up the structure search and when we identify motifs upon stress-based variable-cell relaxations. The most important motifs are the orthorhombic conformers for they are compatible with experimental observations of structure in the crystalline regions. We compute the per unit-cell binding energy

$$E_{\rm bind}(a,b,c) \equiv E^{\rm unit\ cell}_{\rm crystal}(a,b,c) - 2E^{\rm unit\ cell}_{\rm monomer} \tag{1}$$

(or a straightforward generalization when characterizing nonorthorhombic motifs). The elastic response properties, as well as probabilities for finding PVF in an ES, are defined by changes in the binding energy.

A. Finding PVF polymer conformers

To establish a best guess for the GS structure of semicrystalline PVF, we have identified 24 plausible initial guesses, denoted A through X, for a two-chain unit-cell configuration that complies with the experimental finding of PVF having an orthorhombic cell. There are two ways to arrange the pair of zig-zag structures of PE chains [71,77] and more for PVF. The unit cell fits one fluorine atom per PVF chain but these atoms may sit either aligned (at the same along-chain position) or with a relative shift. Moreover, they may have different relative rotations. We refer to the Appendix for a more detailed presentation of our structure-search starting point.

All of these initial guesses, or candidate structures, are subjected to full relaxations (of atoms and of unit-cell parameters), as described by CX. The Appendix and the SM [78] provide a full characterization of these final structures in terms of volume and per-unit-cell binding energy, as well as structure indicators such as significant polarity and unit-cell shape. Some of them break the initially assumed orthorhombic unit-cell shape and several initial guesses end up relaxing to identical motifs. Equivalent unit-cell volumes/shapes, binding energies, and polarization are part of the criteria for considering relaxed candidate structures as one and the same motif. Additional discriminators are whether the along-chain positions of the two fluorine atoms (in each molecular chain) are located at the same c-axis coordinate (as will be identified by a motif subscript p) or relatively shifted (as identified by subscript s), as detailed in the Appendix and in Table S.I of the SM.

B. Validation by energy-mapping and elastic-response characterizations

We characterize the above-described search for structure and binding-energy values of PVF motifs as *full-stress* based. The fact that these calculations proceed with a full unit-cell relaxation (up to our chosen convergence criteria) makes them susceptible to potential convergence, and hence accuracy, problems, at least in plane-wave DFT that we use. Full-stress optimizations are based on the k-point sampling that is judged appropriate for the initial unit-cell geometry. This type of extended-system representation can be misleading if the unit cell incurs significant shape changes. We ameliorate this convergence problem by repeating such variable-cell calculations (restarting at the predicted structure and thus with a continuously updated and increasingly more relevant k-point sampling) until we have full convergence on structure and energies.

We also use (for GS and the first two ES) a safer "map" technique to provide validation for the structure predictions. The underlying challenge of succeeding with the full-stress search lies in the fact that PVF combines exceptionally strong covalent bonds within and along the chains and weaker vdW binding between the chains. The elastic and plastic response of polymer crystals are set by a highly anisotropic stiffness and can be difficult to converge through full-stress relaxations. As further described in the SM [78], the idea of the map structure search is to optimize the unit cell in the direction along the chains (unit-cell direction c) separately from relaxations (in perpendicular unit-cell directions) that reflect the impact of the much weaker interchain noncovalent forces.

Calculation of the elastic coefficients gives us a way to further test the consistency of our stress-based motif search. The set of elastic coefficients defines acoustic modes and thus serves as a check as to whether the identified motifs have any resistance against at least some runaway deformations. We note that for orthorhombic crystals there are nine independent elastic components: C_{11}, C_{22}, C_{33}, C_{12}, C_{13}, C_{23}, C_{44}, C_{55}, and C_{66}.

For a practical motif-structure stability test, we extract the elastic constants by applying strain to the unit cells, while evaluating the volume-specific strain energy. We allow for full atomic relaxations at each deformation increment, because the polymer crystals are not centrosymmetric. This prevents artificially high stiffness emerging as a result of covalent bond stretching. For the orthorhombic GS, ES1, and ES2 motifs, the Born-1 to Born-4 criteria [84,85],

$$C_{11} > 0, \tag{2}$$

$$C_{11}C_{22} - C_{12}^2 > 0, \tag{3}$$

$$C_{11}C_{22}C_{33} + 2C_{12}C_{13}C_{23} - C_{11}C_{23}^2 - C_{22}C_{13}^2 - C_{33}C_{12}^2 > 0 \tag{4}$$

$$\text{for} \quad i \in \{4,5,6\} : C_{ii} > 0, \tag{5}$$

must be satisfied to ensure mechanical stability.

C. Polarization response

For predictions of (soft-matter) spontaneous polarization [86,88] we use a Berry-phase framework [89,90] to track the response to an infinitesimal electrostatic field. To that end, we seek and use a path λ of hypothetical distortions that connects an actual motif with a reference state of vanishing expected spontaneous polarization. The desired reference state (at say $\lambda = 1$) is typically a high-symmetry state. In contrast, the actual motif (at, we assume, $\lambda = 0$) breaks the symmetry so that the material can get a finite polarization P_i in some direction i (if suitably poled and prepared).

Figure 2 illustrates our computational procedure to determine the polarization of the GS and ES PVF motifs. The atoms in the schematics are here shown for the GS PVF motif (and corresponding to an initial twist angle, $\phi = 0^\circ$). Our fluorinated polymers are built from compact monomers

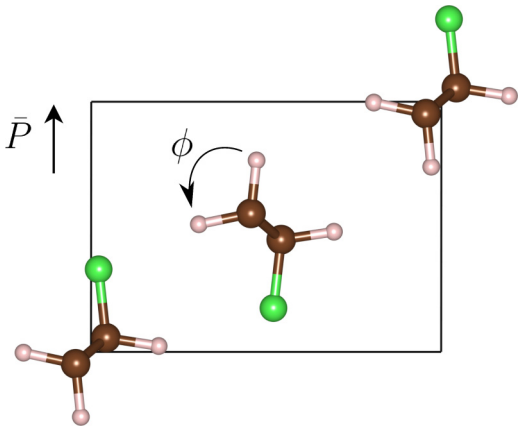

FIG. 2. Schematics of the GS PVF motif and of the computational approach we use to characterize the spontaneous polarization of the GS and ES PVF motifs [4–6,86,87]. For the central chain in any given motif, we define an axis of rotation (aligned with unit-cell vector c) by the center of the carbon atoms. We then apply an increasing twist ϕ selectively to that chain and use the modern theory of polarization to compute the variation in a polarization measure $\Delta P_{i,\mathrm{Berry}}^{\lambda=\phi/180}$. The upwards arrow emphasizes that a considerable polarization (matching the $P \approx 19\ \mu\mathrm{cm}^{-2}$ value previously predicted for β-PVDF [6]) can emerge in the b-unit-cell direction for several of the orthorhombic ES motifs, starting with ES2.

that permit easy chain rotation. We therefore have access to a simple deformation path, by incrementally rotating one chain up to $\phi = \pm 180^\circ$. This is done in an otherwise frozen unit cell.

At any given assumed deformation (in our case, assumed rotational increment $\lambda = \phi/180$), we rely on an assortment of many plane-wave DFT codes, e.g., QUANTUM ESPRESSO (QE) [91,92]: efficient evaluation of a k-space average of the Berry phase associated with the energy bands in solids [90]. This effectively provides us with a mapping of how the node positions of Wannier functions [86] change with the deformation ϕ and thus an unambiguously defined evaluation of a measure $\Delta P_{i,\mathrm{Berry}}^{\lambda=\phi/180}$ of the polarization along a given unit-cell vector direction i [86]. One caveat is that this computed measure is a multivalued function of λ, having branches that differ by integer numbers of the so-called quanta of polarization [88]. However, we can extract the actual spontaneous polarization P_i (in direction i) as the difference given by the extremes of the distortion path:

$$P_i = \left|\Delta P_{i,\mathrm{Berry}}^{\lambda=1} - \Delta P_{i,\mathrm{Berry}}^{\lambda=0}\right|. \tag{6}$$

In practice, we need to ensure that we have consistently stayed on the same polarization branch. We therefore shift, at every λ, the nominal QE polarization result, $\Delta P_{i,\mathrm{Berry}}^{\lambda=\phi/180}$, onto a single branch and then insert the resulting uniquely defined predictions $\tilde{P}_i^{\lambda}$ in the right-hand side of Eq. (6).

Returning to Fig. 2, we note that by symmetry GS PVF must have a vanishing polarization in the b direction, $P_{\mathrm{b}}^{\mathrm{GS}} \approx 0$, because the contribution from chains cancels due to their alternating arrangement of the F atoms. However, the GS structure could have a small $P_{\mathrm{a}}^{\mathrm{GS}}$ value. We compute this value by rotating the central chain, as illustrated, in the GS PVF unit cell, up to $\phi = 180^\circ$. This rotation produces a fictitious state that resembles β-PVDF [4–6] but must have $\tilde{P}_{\mathrm{a}} \approx 0$ by symmetry. As such, that fictitious system can serve as a reference for our prediction of vanishing polarization ($P_{\mathrm{a,b}}^{\mathrm{GS}} \approx 0$) for the GS PVF motif.

As illustrated by the upwards arrow in Fig. 2, however, the orthorhombic ES2, ES6, ES11, and E13 motifs can develop a spontaneous polarization along unit-cell axis b. For example, the ES2 motif exists as a variant (identified and discussed in the Appendix) of the structure that emerges with a $\phi = 180^\circ$ center-chain rotation implemented in Fig. 2. A variant of the structure that is shown in the figure (at $\phi = 0^\circ$) serves as an ES2 reference for computing $P_{\mathrm{b}}^{\mathrm{ES2}}$.

III. COMPUTATIONAL DETAILS

Throughout this paper we use plane-wave DFT from the QE code suite [91–93], together with optimized norm-conserving Vanderbilt (ONCV) pseudopoentials from the SG15-PBE set version 1.2 [94,95]. These contain the complete $2s^2 2p^2$ electron configuration for carbon, $2s^2 2p^5$ for fluorine, and $1s^1$ for hydrogen. To ensure full convergence, we use a kinetic energy cutoff at 2180 eV (160 Ry) with a four times higher cutoff for the density. We use Monkhorst-Pack [96] k-space sampling, centered at the Γ point. Structures are optimized using the Broyden-Fletcher-Goldfarb-Shanno algorithm [97–100] and considered to be converged when the force acting on each atom is smaller than 5×10^{-7} eV/Å.

For the comparison of plausible PVF motifs (see SM [78]) and for mapping of the energy of deformation we use a grid of $4 \times 8 \times 10$ to sample the k space. We conduct the initial convergence test for β-PVDF using a $2 \times 4 \times 10$ mesh, and $4 \times 4 \times 10$ for PE. We map out the unit-cell binding energy variation using a set of constrained unit-cell relaxations.

The Berry phase calculations employ the same k-point mesh as in the unit-cell relaxation, averaging the results over the maximum number of k points allowed by the mesh [86,88].

Unit-cell schematics and mapping of energy variations (reported in the SM [78]) are provided using VESTA [101] and XCRYSDEN [102].

IV. RESULTS AND DISCUSSION

Table I summarizes the properties for GS, ES1, and ES2, the three most energetically favorable structures that remain orthorhombic during these variable-cell relaxations in full-stress evaluations [6]. We denote the lowest binding-energy motif as "GS," as we consider it a plausible guess for the actual (orthorhombic) GS form of would-be fully crystalline PVF. More broadly, we consider the GS, ES1, and ES2 motifs as representative of a well-prepared PVF system at finite temperatures T. They are all orthorhombic and thus both mutually compatible and consistent with experimental observations. The actual mixture of PVF conformers (and their internal polarization state) may reflect the history of the sample preparation.

Figure 3 presents an overview of our predictions for the binding energies and structure features of the GS and for the first set of ES systems. The Appendix (and Table S.II of the SM [78]) reports how these motifs have emerged from initial guesses, sometimes convergent on an identical motif. In Fig. 3

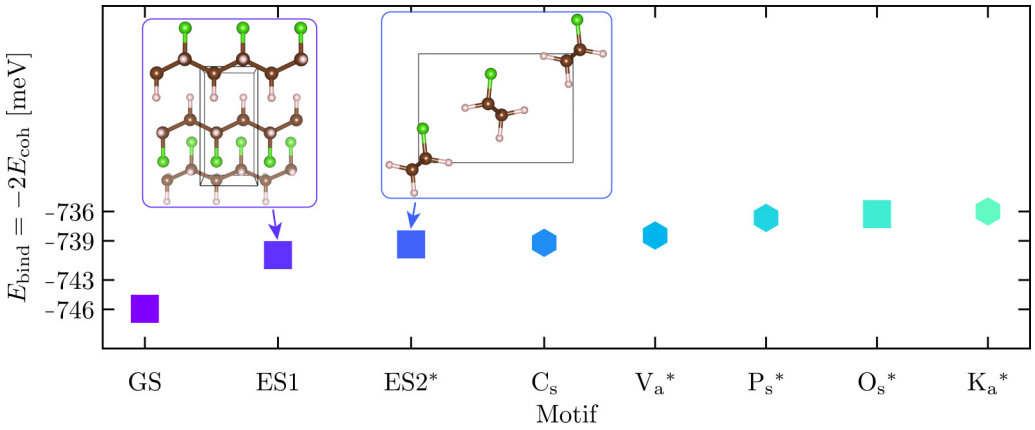

FIG. 3. Summary of (full-stress) PVF-motif structure search and motif identification. We sort the set of fully relaxed motif predictions according to their (per unit-cell) binding-energy values, using an asterisk to identify a pronounced polarization value. We use a square symbol only for those relaxations that lead to an orthorhombic motif, i.e., remain consistent with one of the key experimental inputs we have for the crystalline regions of PVF samples.

we have (apart from GS, ES1, and ES2) kept a reference to the initial-guess labeling to facilitate the comparison. We also mark by a square symbol the cases that remain orthorhombic upon relaxations and by an asterisk those that have a considerable spontaneous polarization.

A. Motif structure description

Table II summarizes and contrasts our full-stress and map (or constrained-stress) structure optimization for PE, β-PVDF, and PVF. The table also provides a comparison with previous structure descriptions, experimental or computational. In all the here-reported studies we have kept a choice for the density of k-point samplings that are consistent with the variation in the system-specific unit-cell extensions.

The top section of Table II provides an overview of experimental characterizations for the PE crystal [103–105,107–109] and a summary of a previous CX-based PE structure characterization [71]. The latter was obtained using ultrasoft pseudopotentials [110,111] with a lower wave-function energy cutoff energy and a less dense k-point sampling. We contrast those results to the characterization in this paper, using norm-conserving ONCV pseudopotentials, a high k-point sampling, and a large cutoff energy. We here find a better agreement with experiments for the a lattice constant.

TABLE I. Summary of the properties of the investigated low energy PVF structures. i.e., ground state (GS) and the most relevant excited-state (ES) conformers; the Appendix, supported by the SM [78], provides a complete listing. All of these are orthorhomic and thus consistent with experimental observations. The table includes the "origin"-structure label (letters), the resulting motif (subscripted letters) and motif sorting (GS/ES no.), the volume of these unit cells, and the difference in the (per unit-cell) binding energy with respect to the ground state ($\Delta E_{\rm bind}$).

Origin	Polar	Volume (Å^3)	Motif	State	$\Delta E_{\rm bind}$ (meV)
G	No	96.095	G_p	GS	0.00
W	No	96.188			0.41
E	No	96.942	D_s	ES1	5.49
D	No	96.817			5.55
L	No	96.831			5.84
I	Yes	96.997	I_s	ES2	6.58
T	Yes	97.048	T_s		6.87

TABLE II. Table of calculated and measured lattice parameters, in Å, for PE, PVDF, and PVF.

System/data type	a_0	b_0	c_0
PE			
Neutrons 4 K[a]	7.121	4.851	2.548
Neutrons 90 K[a]	7.161	4.866	2.546
X-ray diffraction[b]	7.388	4.929	2.539
X-ray diffraction[c]	7.42	4.96	
CX[d]	7.218	5.024	2.553
CX map	7.144	5.044	2.552
CX stress	7.155	5.032	2.552
***β*-PVDF**			
X-ray diffraction[e]	8.47	4.90	2.56
X-ray diffraction[f]	8.58	4.91	2.56
CX map[g]	8.581	4.763	2.575
CX stress[g]	8.579	4.758	2.575
CX stress	8.581	4.752	2.575
PVF			
GS stress	7.265	5.180	2.556
GS map	7.267	5.181	2.556
ES1 stress	7.192	5.272	2.556
ES1 map	7.194	5.274	2.556
ES2 stress	7.341	5.169	2.556
ES2 map	7.346	5.170	2.556

[a]Reference [103].
[b]Measured at 77 K [104].
[c]Measured at 77 K [105].
[d]Reference [71].
[e]Measured at 293 K using thin-film PVDF [31].
[f]Measured at 293 K using thin-film PVDF [106].
[g]Reference [6].

However, there are no discernible changes for b and c values. We ascribe the difference in the a value primarily to the switch to norm-conserving pseudopotentials. We also conclude that we have converged the description of PE with respect to k points.

In the middle section of Table II, we show that by using a corresponding k-point sampling for a CX characterization of β-PVDF, the model provides an excellent description. The herein predicted c lattice constant is essentially spot on, while the a (b) results agree with one of the x-ray diffraction reports (slightly underestimated the x-ray values). In the table we also include results from Ref. [6] obtained using a lower k-point sampling and they too are in excellent agreement. We conclude that with the mutually consistent k-point sampling we have a converged description of both PE and β-PVDF, and may therefore provide reliable predictions for the closely related PVF.

The bottom section of Table II shows our predictions for the unit-cell details of the orthorhombic GS and two metastable conformers, ES1 and ES2, of small excitation energies. The table shows (for each of the key PVF motifs) the results obtained by our standard stress-based relaxation approach, and by the mapping test (summarized in the SM [78]). They agree at the picometer level. We find that the sets of motifs are all orthorhombic (consistent with experimental observations) and have essentially the same lattice constants. These motifs can coexist with 1–2% strain even within the same crystalline block of the overall PVF structure.

B. Elastic coefficients and Born stability

We evaluate the elastic constants associated with the would-be single-crystal elastic response because they are a useful supplement in soft complex matter. Since measurements typically reflect the net elastic response (dominated by the plyable matrix) we need coarse-grained modeling to connect the microscopic and mesoscopic pictures [72,112–115], for example to track, e.g., wear impact on PVF/β-PVDF used in flexible applications. However, having DFT predictions enables the investigation of mechanical stability of the different motifs, and the crystalline components can provide input data to calibrate classical force-field descriptions [71,73,116].

Table III presents our results for the elastic response coefficients for the β-PVDF ground state, as well as for the GS and first two ES motifs of PVF. It is instructive to compare the theoretical elastic constant predictions (for crystalline β-PVDF) with measurements (on a sample that is assumed to be uniaxially orientated, that is, poled) [117,118]. Ultrasonic measurements at $T = 293$ K yield the following results for diagonal (off-diagonal) elasticity components [119]: $C_{11} = 3.61$, $C_{22} = 3.13$, and $C_{33} = 1.63$ GPa ($C_{12} = 1.61$, $C_{13} = 1.42$, and $C_{23} = 1.31$ GPa).

We note that the elastic constants associated with uniaxial normal strain states perpendicular to the chain direction (i.e., C_{11} and C_{22}) are one order of magnitude higher than experimental data. We believe that this discrepancy can be attributed to thermally induced compliance, as the DFT results correspond to 0-K data, and the measurements were conducted at room temperature [119]. Moreover, the theoretical predictions of $C_{33} \approx 300$ GPa for PVF and β-PVDF deviate from the measurements in Ref. [119] by approximately two orders of magnitude. However, the computed results are consistent with experimentally observed elastic constants associated with tensile strains, or propagating sound waves, in the chain direction of PE, where the measured modulus is in excess of 300 GPa (see, e.g., Refs. [120–123]). Similar results were found in Ref. [124], the authors of which performed DFT modeling of β-PVDF based on the PBE XC functional. This is as expected, because the theoretical results pertain to single-crystal problems where the C_{33} reflects the along-chain covalent carbon-carbon bond (unlike the measurements). The covalent carbon-carbon bond is among the strongest in nature, giving, for example, diamond an exceptional hardness. However, the crystalline regions make up only about 50% of the volume in a fluorinated polymer [7,8,27,28] as they are surrounded by a surrounding matrix with rubberlike response properties. The low value for the measured β-PVDF C_{33} coefficient should therefore be interpreted in an entirely different context: It reflects instead an effective (composite-system) elastic response, which is always dominated by the softer component.

TABLE III. Elastic stiffness constants for PVF motifs and for β-PVDF. All elastic-constant values are listed in GPa. The entries for Born-2 and Born-3 criteria are in GPa^2 and GPa^3, respectively; These entries reflect an evaluation of the left-hand-side expressions of Eqs. (3) and (4).

	PVDF	PVF		
	β	GS	ES1	ES2*
C_{11}	23.64	14.70	20.87	13.43
C_{22}	21.46	19.25	12.75	16.10
C_{33}	301.15	318.89	316.64	316.20
C_{12}	2.95	3.75	4.07	5.77
C_{13}	−0.93	0.16	0.04	0.05
C_{23}	0.77	0.91	0.27	1.19
C_{44}	14.33	7.67	24.12	9.14
C_{55}	12.73	27.66	4.80	29.33
C_{66}	27.90	20.18	22.62	19.92
Born 2	500	270	250	183
Born 3	150000	86000	79000	58000

In any case, our elastic-response predictions, Table III, permit us to directly test the mechanical stability of our predicted motifs, and hence the quality of our structure predictions. We do this for both β-PVDF and the three lowest-energy PVF motifs, i.e., cases where the unit cell remains orthorhomic and where we can rely on a simple set of Born criteria, Eqs. (2)–(5). Compliance with all of the Born criteria (for these orthorhombic structures) follows from the fact that the reported determinations of the Born-2 and Born-3 criteria, as well as all C_{ii} entries, are positive and large. Overall, we find that the PVF motifs clear the Born-stability criteria with margins. For the GS case, the criteria are met at a level that approaches that which characterizes β-PVDF (known to be metastable).

C. Polarization response

A crystalline and poled sample of the PVF ES2 conformer can be expected to have a polarization in the *b*-axis direction because the motif resembles the β-PVDF structure (compare the second inset of Fig. 3 and the third panel of Fig. 1). Figure S3 of the SM [78] shows a schematics of a pure-PVF-ES2 crystal containing a polarization boundary, i.e., a case where the left (right) domain has a downward (upward) pointing spontaneous polarization, given the polar nature of the F-C bond. Application of an upward-pointing electrical field lowers the energy of the ES2 configuration of the latter domain which may therefore grow and produce also a macroscopic polarization change in such a PVF ES2 system. However, for this to happen the local chains must overcome transition barriers for flippling 180° relative to the chains in its immediate surroundings.

Accordingly, our finding of a significant spontatenous polarization for the ES2 conformer does not necessarily imply that PVF may find usage as an actual flexible finite-temperature ferroelectrics. We have shown (to be reported in a forthcoming paper) that PVF and β-PVDF have comparable plastic-deformation properties as asserted in terms of slip mechanisms [76]. However, one needs an elaborate modeling to assertain whether (1) a moderate electric field can, in fact, reverse the polarization (as it can do in β-PVDF) and (2) the expected net spontaneous polarization of a room-temperature PVF system is large enough to serve as an interesting alternative to β-PVDF. Below, we merely provide a cruder modeling to discuss these questions and thus give an impression of the would-be PVF promise as a flexible polarization material.

First, we observe that reversing the polarization is not likely to require larger fields in PVF than in PVDF. Figures S4 and S5 of the SM [78] report a supercell study of the energy cost associated with a selective chain rotation, contrasting GS PVF and PVDF. The approach is similar to what is illustrated in Fig. 2, but now we permit relaxations of neighboring chains. Our paper shows that a twist excitation (make one chain rotate 180° to better align with a reversed external-electric-field direction) has a lower barrier (0.5 eV) in PVF than the energy cost (0.81 eV) that we compute is required in β-PVDF. We interpret the difference between PVF and PVDF twist-excitation energies as indicative of the difference in the PVF and PVDF energy scales for electric-field control. We thus find it plausible that any would-be polarization of PVF would be at least as easy to reverse as it is in β-PVDF.

Figure 4 shows details of our predictions for the spontaneous electric polarization in PVF motifs. The set of black dots in Fig. 4 comprises the calculated $P_{\rm b}^{\phi}$ values. These data fall on various branches of the Berry-phase polarization description, each branch separated by one or more quanta of the along-*b*-axis polarization [86]. However, only one of these branches corresponds to the nonpolar behavior that is expected by symmetry at $\phi = \pm 180^\circ$ (for the case in question). By shifting all data onto that one branch, it is possible to construct an estimate for the spontaneous polarization $\tilde{P}_b^{\phi}$ (gray dotted curve) and compute the spontaneous polarization as $P_b = |\tilde{P}_b^{\phi=0} - \tilde{P}_b^{\phi=180}|$.

Table IV reports P_b polarization results for the set of (the experimentally relevant) orthorhombic conformers of PVF.

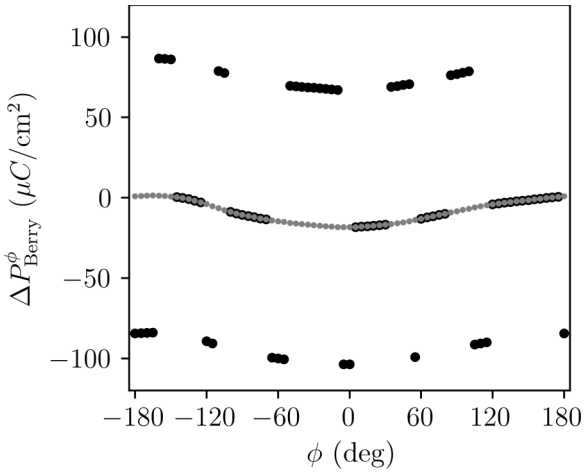

FIG. 4. Calculation of the spontaneous electric polarization (along unit-cell axis *b*) $P_b \approx 19\ \mu{\rm C/cm}^2$ of PVF motif ES2. We use the modern Berry-phase scheme [4–6,86] to track changes in a multivalued measure $\Delta P^{\phi}_{\rm Berry}$ of this polarization as a function of the assumed rotation ϕ of one polymer chain relative to the other inside the ES2 unit cell (bottom panel of Fig. 1). The actual ES2 configuration corresponds to $\phi = 0^\circ$ whereas symmetry implies that the modified structure at $\phi = \pm 180^\circ$ serves us as a nonpolar reference. The set of black dots represents individual $\Delta P^{\phi}_{\rm Berry}$ calculations that fall on one of a range of equivalent branches. The gray dotted curve shows how we collect these calculated data to extract the variation with rotation angle of the actual spontaneous polarization $\tilde{P}_b^{\phi}$. Because this curve goes through the expected $\tilde{P}_b^{\phi=180} \approx 0$ value, we trust it to also predict the ES2 polarization as $P_b \equiv |\tilde{P}_b^{\phi=0} - \tilde{P}_b^{\phi=180}|$.

For some of the higher-energy conformer excitations (with spontaneous polarization in unit-cell direction *a*) we only provide estimates of the polarization. Those estimates are based on the structural similarity with ES2 and ES13 (noting also that the density of polarization contributions is reduced). For a GS PVF crystal (existing at vanishing temperature $T \to 0$) the polarization must disappear and we expect that the computed values, $|P^{\rm GS}_{a,b}| < 0.5\ \mu{\rm C\,cm}^{-2}$, may well be just be a consequence of numerical noise. For the ES2 motif, we predict

TABLE IV. Spontaneous polarization of the PVF GS candidate and of the metastable orthorhombic conformations, in $\mu{\rm C\,cm}^{-2}$; Values in parentheses arise instead in unit-cell directions *a* and are estimated (see text). For each conformer we also list the associated (per-monomer) excitation energy, ΔE_i, relative to the GS, in meV. We combine these data to establish an upper theory-based limit $\langle P\rangle(293)$ for the PVF spontaneous polarization at room temperature, assuming an orthorhombic structure.

	P_b	$\tilde{P}_b^0$	$\tilde{P}_b^{180}$	ΔE_i
GS	∼0	−0.4	−1.0	0
ES1	4	3.4	−0.5	5.6
ES2	19	18.2	−1.3	6.7
ES6	(12)			9.7
ES11	(12)			17.2
ES13	17	17.7	0.3	22.8
		$\langle P\rangle(293) = 3.5$		

the spontaneous polarization to be $P_b \approx 19\ \mu C\,cm^{-2}$ along unit-cell axis b (see Table IV). This value is comparable to that predicted for β-PVDF, 19 $\mu C\,cm^{-2}$ [6]. The β-PVDF theory value is substantially higher than the actual measured polarization value of 10 $\mu C\,cm^{-2}$ obtained by circuit measurements for solid-state coextruded films β-PVDF [125]. Such theory-experiment differences are expected also for PVF, since one cannot expect a perfectly crystalline preparation. Because the crystallinity of semicrystalline PVF is about 50%, we anticipate that the practical polarization limit for PVF will likely not exceed 50% of that computed.

For PVF, we find that there is only a small difference in the per unit-cell energy of different orthorhombic motifs in relation to the GS motif. Table S.I of the SM [78] reveals that the volume differences do not exceed 1% when switching among these mutually compatible low-energy orthorhombic conformers. It is therefore possible that some of these motifs will coexist in a crystalline block of the PVF system.

To compute an upper (theoretical) limit for the PVF polarization at finite temperature, we resort to equilibrium statistical mechanics. This treatment is subject to the experimental observation that the crystalline blocks are orthorhombic. For the orthorhombic motifs (GS, ES1, ES2, ES6, ES11, and ES13 identified in Table S.I of the SM [78]) we find increasing per-unit-cell binding energies,

$$E_{i=0} = E_{\rm GS} = E_{\rm bind,GS}, \tag{7}$$

$$E_i = E_{{\rm ES}i} = E_{{\rm bind,ES}i}, \tag{8}$$

and per-unit-cell motif-excitation energies,

$$\Delta E_i = E_i - E_{i=0}, \tag{9}$$

that are smaller than k_BT at room temperature (≈25.25 meV).

In a dramatic approximation, we may consider each orthorhombic-conformer unit cell as loosely coupled, each being an independent subsystem with a polarization P_b^i specific for the motif. We may then assign Gibbs-free energy weights [126,127],

$$g_i(T) = \frac{e^{-\Delta E_i/k_BT}}{\sum_j e^{-\Delta E_j/k_BT}}, \tag{10}$$

and arrive at an upper-limit estimate for the polarization using

$$\langle P\rangle(T) = \sum_{i\geqslant 0} g_i(T) P_b^i. \tag{11}$$

For a PVF crystalline region, at room temperature, a plausible upper-limit estimate $\langle P\rangle(293) = 3.5\ \mu C\,cm^{-2}$ emerges when we limit the sum in Eq. (11) to $i \leqslant 2$ (thus including only the GS, ES1, and ES2 conformers). For comparison, if we were, in fact, to treat each unit cell as a nearly decoupled subsystem (i.e., include all orthorhombic conformers with nonzero spontaneous polarization P_b in Eq. (11) with the stated weights) the upper-limit estimate would instead become $\langle P'\rangle = 5\ \mu C\,cm^{-2}$. However, the local PVF structures in neighboring unit cells cannot rapidly change given the strength of the covalent carbon-carbon bond. It is unclear how large the structural coherence length is in PVF, but the zig-zag line of carbon atoms in a chain is unable to rotate or alter its registry relative to neighboring chains at every 2.56 Å repetition period along unit-cell direction c. Treating each unit cell as a subsystem (as implicitly done in $\langle P'\rangle$) overestimates the entropy and consequently also the importance of structural variations at room temperature. This suggests that the 3.5 $\mu C\,cm^{-2}$ value is the more relevant upper-limit estimate, although that too is based on a crude model.

Nevertheless, from the statistical-ensemble analysis we conjecture that (1) PVF *may* be poled to have a small net polarization at room temperatures and (2) the best-possible PVF polarization value remains considerably smaller than the best-possible β-PVDF (single-crystal) value, predicted theoretically at 19 $\mu C\,cm^{-2}$ [6]. We also observe that our finding of many nearly degenerate PVF polymer conformers suggests that a would-be PVF polarization will depend critically on sample preparation.

V. SUMMARY AND CONCLUSION

We apply first-principle DFT with a nonempirical, vdW-inclusive functional to explore the orthorhombic phases of two partially fluorinated analogs of PE: PVDF and primarily PVF. For PVF, there is synthesis but incomplete experimental characterization. It must therefore be considered a complex matter problem: We do not fully know the structure and have no direct way to use DFT to predict properties.

Accordingly we have worked to first identify the PVF structure and then to predict properties (binding energy, lattice constants, elastic response, as well as the spontaneous polarization value). This is done by identifying a set of relevant initial guesses for the orthorhombic PVF structure and by tracking variable-cell and atomic relaxation using the CX functional.

We find a plausible orthorhombic GS structure for PVF with lattice constants $a = 7.26$ Å, $b = 5.18$ Å, and $c = 2.55$ Å, similar to that of β-PVDF and PE. We also determine the elastic stiffness constants of the PVF GS to validate our structure predictions for the motifs, using a set of Born criteria that we find satisfied to about the same extent that they are for the related β-PVDF.

Finally, with the structure determined and analyzed, we compute the polarization response and find that it vanishes in GS PVF and may at most rise to a moderate value at room temperatures (because PVF does have low-energy conformers that are polar). We find that even under ideal conditions, it is unlikely that PVF can match the good spontaneous-polarization properties that are known for the closely related β-PVDF systems.

ACKNOWLEDGMENTS

Work was supported by the Swedish Research Council (VR), through Grants No. 2018-03964, No. 2022-03277, No. 2016-04162, and No. 2022–04497; the Swedish Foundation of Strategic research, through Grants No. IMF17-0324 and No. SM17-0020; Sweden's Innovation Agency Vinnova, through Project No. 2020-05179; and the Chalmers Area-of-Advance Production. The authors also acknowledge computer-time allocations from the Swedish National Infrastructure for Computing under Contracts No. SNIC2019-2-19, No. SNIC 2020-3-13, No. SNIC2021-3-18, No. SNIC-2022-

3-16, No. SNIC-2021/6-287, No. SNIC-2022/6-286, and No. NAISS-2023-3-22, as well as from storage allocation NAISS-2023-6-326. The authors furthermore acknowledge allocations from the Chalmers Centre for Computing, Science, and Engineering (C3SE).

APPENDIX: STRUCTURAL MOTIFS PVF GROUND STATE

We use the efficiency of modern DFT codes like QE to address the soft-complex-matter challenge of PVF. It is a soft-matter problem for while there are strong covalent-ionic bonds within and along the chains, they are held together by a competition between vdW attraction and steric hindrance. It is a soft-complex-matter problem for while it is known that PVF is orthorhombic, there are no single-crystal samples to fully reveal the structure of the lowest-energy unit cell(s).

Our solution strategy is to focus on understanding the details of a would-be PVF single crystal, be it for the lowest-binding-energy GS or an ES conformer. The paper thus involves defining a database of plausible PVF motifs. The overall idea is to use DFT to accurately compute and implement relaxations specified by associated predictions of forces and stresses [128]. In essence, we adopt an idea that has been used early for a computational search for metastable alumina phases [20], and in turn to predictions of alumina surface terminations [129–131], of seeded growth [132,133], and of graphane stacking [81]. In those problems the forces are all strong and of a covalent-ionic nature. Here, we require a vdW-inclusive DFT (such as the CX functional that we use) and for which QE permits both full-stress and constrained-stress implementations of variable-cell calculations [6,128,134]. A vdW-inclusive prediction of CO_2 adsorption in functionalized metal-organic frameworks [21] provides a related example of addressing soft-complex-matter challenges by using DFT-based predictions for relaxations. However, we may now also have dramatic changes in the basic structure (as indeed found for some PVF motifs).

In practice, we define a set of candidate structures (initial guesses for the PVF unit-cell structure that are inspired by the also orthorhombic PE and β-PVDF crystals) and—upon full relaxations in the parameter-free CX functional—we identify and prune redundancies to define actual PVF motifs. Finally we sort by their predicted binding energies to find a plausible guess for the GS structure as well as relevant ES PVF conformers. The latter are the set of motifs that (like GS) retains the orthorhombic unit-cell geometry and have an energy sufficiently close to that of the GS, so they may coexist in actual PVF at room temperature.

Figure 5 shows a schematic of how we set up 24 candidate structures, with labels *A* through *X*. They start out in orthorhombic unit cells (before we turn on CX relaxations). All of these initial guesses contain two CFH-CH_2 units, one per chain. However, half of them have the F-atom position shifted between the chains and half of them have (initially) the F atoms sitting aligned at the same along-chain (*c*) coordinate. What is important is where these initial systems land when relaxations define a set of 16 motifs (see below). With regard to the relative F-atom positions, some motifs remain or become "shifted" (earning a subscript *s*) and some have a same-*c*-plane organization (earning a subscript *p*).

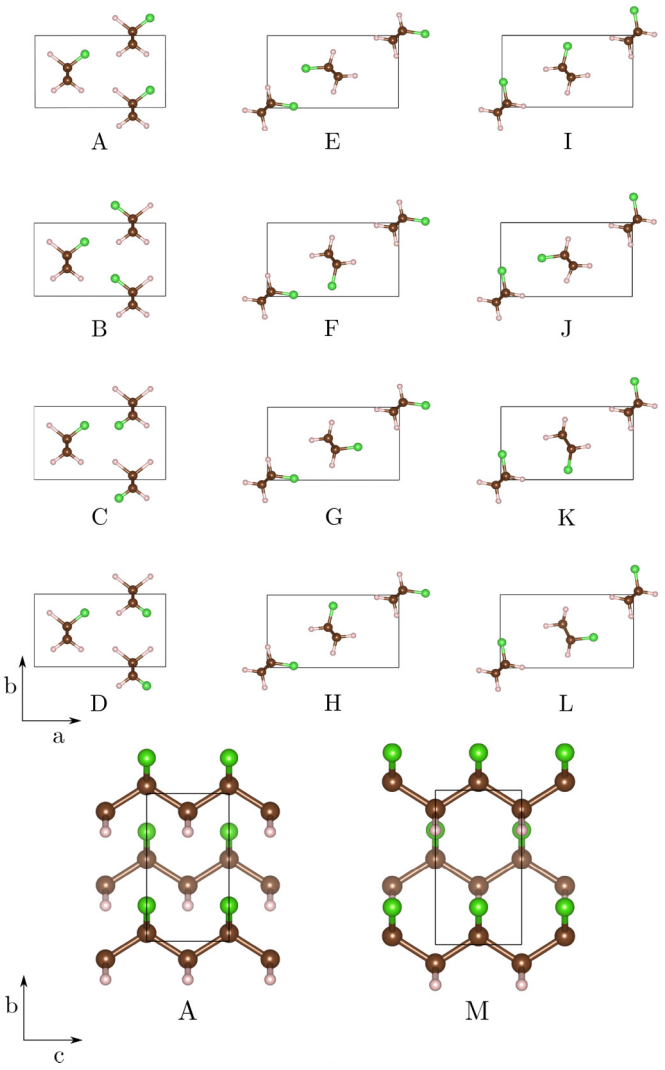

FIG. 5. Initial structure guesses for two-PVF-chain unit-cell structures that upon relaxation produce actual PVF motifs. The latter are in turn candidates for the set of relevant PVF crystalline conformers. We consider different relative F-atom placements on the two chains and subsequent rotations of one chain relative to the other (upper group of panels). Initial guesses A through L (M through X) consider such cases when the F-atom position on each chain is shifted one-half unit-cell vector *c* from (is aligned with) the other, as illustrated in the lower left (right) panel.

Table S.I of the SM [78] lists, for every initial guess, a set of characteristic properties of these PVF states. It is an overcomplete motif-candidate collection, where we use the label subscript (*p* or *s*) according to the relative position of the F atoms and a superscript to identify whether we can expect a significant polarization. We also there record the final-state unit-cell symmetry, volume, and total-binding energy. We group them into combined motifs (as also reflected in the table) if (1) their energy differences are within 0.5 meV and the volume differences are smaller than 0.1 $Å^3$, if (2) the polar/structure discriminators agree, and if (3) we can find a transformation (a combination of unit-cell translation, reflection, or rotation) that relates the structure seen in one

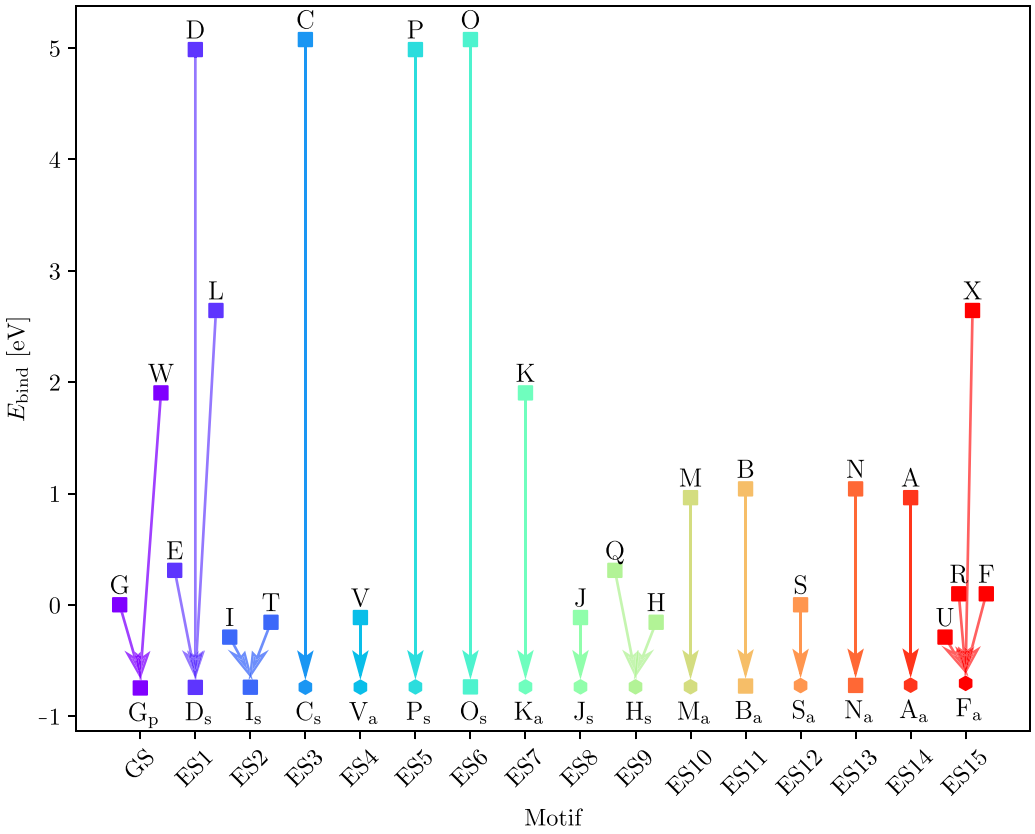

FIG. 6. Energetics of relaxation for the set of PVF motifs that leads to our prediction for a plausible GS and for related metastable polymer conformers. The Appendix discusses the nature and structure of these motifs or initial guesses. The *y* axis shows the polymer binding energy, Eq. (1), as predicted in CX calculations under full variable-cell and atomic relaxations.

final case with that of another. We caught significant redundancy for what we identified as GS, ES1, and ES2, and some for higher-energy motifs, denoted ES3-ES15. Except for the ES3 member, the energy difference to GS is larger in the latter groups. ES3 and several of the higher-energy motifs are nonorthorhombic and therefore not structurally compatible with observations, nor with our GS motif. We ignore these motifs in our finite-temperature modeling.

Figure 6 reports an overview of binding-energy changes that arise as initial-guess structures relax into actual motifs. Different initial guesses do evolve into the same motifs and a significant part of the paper is that of pruning for redundancy after our "motif-production" stage (see SM [78]). We name those by the letter (for example *G* for what turned out to be the GS motif) of the first-labeled initial guess that produced it. Once we have ensured full unit-cell and atomic relaxations, we order the resulting motifs by increasing energies as GS, ES no., i.e., the label for our figure ordinate. Also, we use a square symbol to identify those structures (initial guess or motifs) that are orthorhombic (as is actual PVF).

[1] B. Ameduri, Fluoropolymers: The right material for the right applications, Chem. Eur. J. **24**, 18830 (2018).

[2] E. Leivo, T. Wilenius, T. Kinos, P. Vuoristo, and T. Mäntylä, Properties of thermally sprayed fluoropolymer PVDF, ECTFE, PFA and FEP coatings, Prog. Org. Coat. **49**, 69 (2004).

[3] M. G. Dhara and S. Banerjee, Fluorinated high-performance polymers: Poly(arylene ether)s and aromatic polyimides containing trifluoromethyl groups, Prog. Polym. Sci. **35**, 1022 (2010).

[4] F. Pelizza, B. Smith, and K. Johnston, A van der Waals density functional theory study of poly(vinylidene difluoride) crystalline phases, Eur. Phys. J.: Spec. Top. **225**, 1733 (2016).

[5] F. Pelizza and K. Johnston, A density functional theory study of poly(vinylidene difluoride) crystalline phases, Polymer **179**, 121585 (2019).

[6] C. M. Frostenson, E. J. Granhed, V. Shukla, P. A. T. Olsson, E. Schröder, and P. Hyldgaard, Hard and soft materials: Putting consistent van der Waals density functionals to work, Electron. Struct. **4**, 014001 (2022).

[7] R. Large, W. Maddams, and J. Preedy, X-ray-diffraction pole figure measurements on a poly(vinyl fluoride) film, J. Appl. Polym. Sci. **22**, 3031 (1978).

[8] G. Natta, Macromolecular Chemistry: From the stereospecific polymerization to the asymmetric autocatalytic synthesis of macromolecules, Science **147**, 261 (1965).

[9] M. Bozorg, A. Altomare, and K. Loos, Synthesis of polyvinylidene fluoride and its copolymers, in *Organic Ferroelectric Materials and Applications*, Woodhead Publishing Series in Electronic and Optical Materials, edited by K. Asadi (Woodhead Publishing, Cambridge, MA, 2022), pp. 85–112.

[10] B. Ameduri and B. Boutevin, *Well-Architectured Fluoropolymers: Synthesis, Properties and Applications* (Elsevier, Oxford, 2004).

[11] A. L. Moore, Fluoroelastomer composition and properties, in *Fluoroelastomers Handbook*, Plastics Design Library, edited by A. L. Moore, 2nd ed. (William Andrew, Norwich, NY, 2006), pp. 13–22.

[12] J. G. Drobny, Fluoroelastomer composition and properties, in *Fluoroelastomers Handbook, Plastics Design Library*, edited by J. G. Drobny, 2nd ed. (William Andrew, Norwich, NY, 2016), pp. 17–26.

[13] H. Kawai, The piezoelectricity of poly (vinylidene fluoride), Jpn. J. Appl. Phys. **8**, 975 (1969).

[14] B. Ameduri, From vinylidene fluoride (VDF) to the applications of VDF-containing polymers and copolymers: Recent developments and future trends, Chem. Rev. **109**, 6632 (2009).

[15] V. Cardoso, D. Correia, C. Ribeiro, M. Fernandes, and S. Lanceros-Méndez, Fluorinated polymers as smart materials for advanced biomedical applications, Polymers **10**, 161 (2018).

[16] J. J. Reisinger and M. A. Hillmyer, Synthesis of fluorinated polymers by chemical modification, Prog. Polym. Sci. **27**, 971 (2002).

[17] K. Nakamura, M. Nagai, T. Kanamoto, Y. Takahashi, and T. Furukawa, Development of oriented structure and properties on drawing of poly(vinylidene fluoride) by solid-state coextrusion, J. Polym. Sci. Part B: Polym. Phys. **39**, 1371 (2001).

[18] A. Itoh, Y. Takahashi, T. Furukawa, and H. Yajima, Solid-state calculations of poly(vinylidene fluoride) using the hybrid DFT method: Spontaneous polarization of polymorphs, Polym. J. **46**, 207 (2014).

[19] F.-C. Sun, A. M. Dongare, A. D. Asandei, S. Pamir Alpay, and S. Nakhmanson, Temperature dependent structural, elastic, and polar properties of ferroelectric polyvinylidene fluoride (PVDF) and trifluoroethylene (TrFE) copolymers, J. Mater. Chem. C **3**, 8389 (2015).

[20] Y. Yourdshayan, C. Ruberto, M. Halvarsson, L. Bengtsson, V. Langer, B. I. Lundqvist, S. Ruppi, and U. Rolander, Theoretical structure determination of a complex materials: κ-Al_2O_3, J. Am. Ceram. Soc. **82**, 1365 (1999).

[21] J.-H. Lee, P. Hyldgaard, and J. B. Neaton, An assessment of density functionals for predicting CO_2 adsorption in diamine-functionalized metal-organic frameworks, J. Chem. Phys. **156**, 154113 (2022).

[22] S. Ebnesajjad and P. R. Khaladkar, Introduction to Fluoropolymers, in *Fluoropolymers Applications in the Chemical Processing Industries*, edited by S. Ebnesajjad and P. R. Khaladkar (William Andrew, Norwich, NY, 2005), pp. 1–6.

[23] Y.-Y. Peng, S. Srinivas, and R. Narain, Nature and molecular structure of polymers, in *Polymer Science and Nanotechnology*, edited by R. Narain (Elsevier, Amsterdam, 2020), pp. 13–19.

[24] P. J. Flory, *Principles of Polymer Chemistry* (Cornell University, Ithaca, NY, 1953).

[25] R. J. Young and P. A. Lovell, *Introduction to Polymers* (CRC, Boca Raton, FL, 2011), pp. 545–550.

[26] R. Dallaev, T. Pisarenko, D. Sobola, F. Orudzhev, S. Ramazanov, and T. Trčka, Brief review of PVDF properties and applications potential, Polymers **14**, 4793 (2022).

[27] J. L. Koenig and F. J. Boerio, RAMAN scattering in poly(vinyl fluoride), Die Makromolekulare Chemie **125**, 302 (1969).

[28] R. Golike, Symmetry and dimensions of the crystalline unit cell of polyvinyl fluoride, J. Polym. Sci. **42**, 583 (1960).

[29] J. Hong, J. Lando, J. Koenig, S. Chough, and S. Krimm, Normal-mode analysis of infrared and Raman spectra of poly(vinyl fluoride), Vibrational Spectroscopy **3**, 55 (1992).

[30] J. L. Koenig and J. J. Mannion, Infrared study of poly(vinyl fluoride), J. Polym. Sci. A-2: Polym. Phys. **4**, 401 (1966).

[31] J. B. Lando, H. G. Olf, and A. Peterlin, Nuclear magnetic resonance and x-ray determination of the structure of poly(vinylidene fluoride), J. Polym. Sci., Part A-1: Polym. Chem. **4**, 941 (1966).

[32] G. Zerbi and G. Cortili, Structure of poly-(vinyl fluoride) from its infrared spectrum, Spectrochimica Acta Part A: Molecular Spectroscopy **26**, 733 (1970).

[33] M. Rubinstein and R. H. Colby, *Polymer Physics* (Oxford University, London, 2003).

[34] W. Hu, *Polymer Physics: A Molecular Approach* (Springer, New York, 2013).

[35] W. Callister and D. Rethwisch, *Materials Science and Engineering: An Introduction* (Wiley, New York, 2018).

[36] A. Pribram-Jones, D. A. Gross, and K. Burke, DFT: A theory full of holes? Annu. Rev. Phys. Chem. **66**, 283 (2015).

[37] R. O. Jones, Density functional theory: Its origins, rise to prominence, and future, Rev. Mod. Phys. **87**, 897 (2015).

[38] X. Wu, M. C. Vargas, S. Nayak, V. Lotrich, and G. Scoles, Towards extending the applicability of density functional theory to weakly bound systems, J. Chem. Phys. **115**, 8748 (2001).

[39] S. Grimme, Accurate description of van der Waals complexes by density functional theory including empirical corrections, J. Comput. Chem. **25**, 1463 (2004).

[40] S. Grimme, Semiempirical hybrid density functional with perturbative second-order correlation, J. Chem. Phys. **124**, 034108 (2006).

[41] P. L. Silvestrelli, Van der Waals interactions in DFT made easy by Wannier functions, Phys. Rev. Lett. **100**, 053002 (2008).

[42] A. Tkatchenko and M. Scheffler, Accurate molecular van der Waals interactions from ground-state electron density and free-atom reference data, Phys. Rev. Lett. **102**, 073005 (2009).

[43] P. L. Silvestrelli, van der Waals interactions in density functional theory using wannier functions, J. Phys. Chem. A **113**, 5224 (2009).

[44] S. Grimme, J. Antony, S. Ehrlich, and H. Krieg, A consistent and accurate *ab initio* parametrization of density functional dispersion correction (DFT-D) for the 94 elements H-Pu, J. Chem. Phys. **132**, 154104 (2010).

[45] O. A. von Lilienfeld and A. Tkatchenko, Two- and three-body interatomic dispersion energy contributions to binding in molecules and solids, J. Chem. Phys. **132**, 234109 (2010).

[46] S. Grimme, S. Ehrlich, and L. Goerigk, Effect of the damping function in dispersion corrected density functional theory, J. Comput. Chem. **32**, 1456 (2011).

[47] V. G. Ruiz, W. Liu, E. Zojer, M. Scheffler, and A. Tkatchenko, Density-functional theory with screened van der Waals interactions for the modeling of hybrid inorganic-organic systems, Phys. Rev. Lett. **108**, 146103 (2012).

[48] A. Tkatchenko, R. A. DiStasio, R. Car, and M. Scheffler, Accurate and efficient method for many-body van der Waals interactions, Phys. Rev. Lett. **108**, 236402 (2012).

[49] M. Kim, W. J. Kim, T. Gould, E. K. Lee, S. Lebeque, and H. Kim, uMBD: A materials-ready dispersion correction that uniformly treats metallic, ionic, and van der Waals bonding, J. Am. Chem. Soc. **142**, 2346 (2020).

[50] A. C. Maggs and N. W. Ashcroft, Electronic fluctuation and cohesion in metals, Phys. Rev. Lett. **59**, 113 (1987).

[51] K. Rapcewicz and N. W. Ashcroft, Fluctuation attraction in condensed matter: A nonlocal functional approach, Phys. Rev. B **44**, 4032 (1991).

[52] D. C. Langreth and S. H. Vosko, Exact electron-gas response functions at high density, Phys. Rev. Lett. **59**, 497 (1987).

[53] D. C. Langreth and S. H. Vosko, Response functions and nonlocal approximations, Adv. Quantum. Chem. **21**, 175 (1990).

[54] Y. Andersson, D. C. Langreth, and B. I. Lundqvist, van der Waals interactions in density-functional theory, Phys. Rev. Lett. **76**, 102 (1996).

[55] H. Rydberg, B. I. Lundqvist, D. C. Langreth, and M. Dion, Tractable nonlocal correlation density functionals for flat surfaces and slabs, Phys. Rev. B **62**, 6997 (2000).

[56] H. Rydberg, M. Dion, N. Jacobson, E. Schröder, P. Hyldgaard, S. I. Simak, D. C. Langreth, and B. I. Lundqvist, Van der Waals density functional for layered structures, Phys. Rev. Lett. **91**, 126402 (2003).

[57] M. Dion, H. Rydberg, E. Schröder, D. C. Langreth, and B. I. Lundqvist, Van der Waals density functional for general geometries, Phys. Rev. Lett. **92**, 246401 (2004).

[58] J. Klimeš, D. R. Bowler, and A. Michaelides, van der Waals density functionals applied to solids, Phys. Rev. B **83**, 195131 (2011).

[59] O. A. Vydrov and T. Van Voorhis, Nonlocal van der Waals density functional: The simpler the better, J. Chem. Phys. **133**, 244103 (2010).

[60] J. Wellendorff, K. T. Lundgaard, A. Møgelhøj, V. Petzold, D. D. Landis, J. K. Nørskov, T. Bligaard, and K. W. Jacobsen, Density functionals for surface science: Exchange-correlation model development with Bayesian error estimation, Phys. Rev. B **85**, 235149 (2012).

[61] T. Thonhauser, S. Zuluaga, C. A. Arter, K. Berland, E. Schröder, and P. Hyldgaard, Spin signature of nonlocal correlation binding in metal-organic frameworks, Phys. Rev. Lett. **115**, 136402 (2015).

[62] E. Schröder, V. R. Cooper, K. Berland, B. I. Lundqvist, P. Hyldgaard, and T. Thonhauser, The vdW-DF family of non-local exchange-correlation functionals, in *Non-Covalent Interactions in Quantum Chemistry and Physics: Theory and Applications*, edited by A. O. de la Roza and G. Di Labio (Elsevier, Amsterdam, 2017).

[63] K. Berland, Y. Jiao, J.-H. Lee, T. Rangel, J. B. Neaton, and P. Hyldgaard, Assessment of two hybrid van der Waals density functionals for covalent and noncovalent binding of molecules, J. Chem. Phys. **146**, 234106 (2017).

[64] D. Chakraborty, K. Berland, and T. Thonhauser, Next-generation nonlocal van der Waals density functional, J. Chem. Theory Comput. **16**, 5893 (2020).

[65] V. Shukla, Y. Jiao, C. M. Frostenson, and P. Hyldgaard, vdW-DF-ahcx: A range-separated van der Waals density functional hybrid, J. Phys.: Condens. Matter **34**, 025902 (2022).

[66] T. Thonhauser, V. R. Cooper, S. Li, A. Puzder, P. Hyldgaard, and D. C. Langreth, van der Waals density functional: Self-consistent potential and the nature of the van der Waals bond, Phys. Rev. B **76**, 125112 (2007).

[67] P. Hyldgaard, K. Berland, and E. Schröder, Interpretation of van der Waals density functionals, Phys. Rev. B **90**, 075148 (2014).

[68] P. Hyldgaard, Y. Jiao, and V. Shukla, Screening nature of the van der Waals density functional method: A review and analysis of the many-body physics foundation, J. Phys.: Condens. Matter **32**, 393001 (2020).

[69] T. Jenkins, K. Berland, and T. Thonhauser, Reduced-gradient analysis of van der Waals complexes, Electron. Struct. **3**, 034009 (2021).

[70] V. Shukla, Y. Jiao, J.-H. Lee, E. Schröder, J. B. Neaton, and P. Hyldgaard, Accurate nonempirical range-separated hybrid van der Waals density functional for complex molecular problems, solids, and surfaces, Phys. Rev. X **12**, 041003 (2022).

[71] P. A. T. Olsson, E. Schröder, P. Hyldgaard, M. Kroon, E. Andreasson, and E. Bergvall, *Ab initio* and classical atomistic modelling of structure and defects in crystalline orthorhombic polyethylene: Twin boundaries, slip interfaces, and nature of barriers, Polymer **121**, 234 (2017).

[72] P. A. T. Olsson, P. J. in 't Veld, E. Andreasson, E. Bergvall, E. Persson Jutemar, V. Petersson, G. C. Rutledge, and M. Kroon, All-atomic and coarse-grained molecular dynamics investigation of deformation in semi-crystalline lamellar polyethylene, Polymer **153**, 305 (2018).

[73] P. A. T. Olsson and E. Bergvall, Atomistic investigation of functionalized polyethylene-alumina interfacial strength and tensile behaviour, Comput. Mater. Sci. **187**, 110075 (2021).

[74] K. Berland and P. Hyldgaard, Exchange functional that tests the robustness of the plasmon description of the van der Waals density functional, Phys. Rev. B **89**, 035412 (2014).

[75] K. Berland, C. A. Arter, V. R. Cooper, K. Lee, B. I. Lundqvist, E. Schröder, T. Thonhauser, and P. Hyldgaard, van der Waals density functionals built upon the electron-gas tradition: Facing the challenge of competing interactions, J. Chem. Phys. **140**, 18A539 (2014).

[76] C. M. Frostenson, Facing complex soft matter: tools, validation, and case studies, Ph.D. thesis, Department of Microtechnology and Nanoscience(MC2), Chalmers University of Technology, Göteborg, Sweden, 2024.

[77] P. A. T. Olsson, P. Hyldgaard, E. Schröder, E. P. Jutemar, E. Andreasson, and M. Kroon, *Ab initio* investigation of monoclinic phase stability and martensitic transformation in crystalline polyethylene, Phys. Rev. Mater. **2**, 075602 (2018).

[78] See Supplemental Material at http://link.aps.org/supplemental/10.1103/PhysRevMaterials.8.115603 for details on the PVF structure search, validation of motifs found by that structure search, and determination and comparison of PVDF and PVF energy scales for reversal of the polarization.

[79] S. Woodley, G. M. Day, and R. Catlow, Structure prediction of crystals, surfaces and nanoparticles, Philos. Trans. R. Soc. A **378**, 20190600 (2020).

[80] E. D. Sødahl, S. Seyedraoufi, C. H. Görbitz, and K. Berland, Ferroelectric crystals of globular molecules: Cambridge structural database mining and computational assessment, Cryst. Growth Des. **23**, 8607 (2023).

[81] J. Rohrer and P. Hyldgaard, Stacking and band structure of van der Waals bonded graphane multilayers, Phys. Rev. B **83**, 165423 (2011).

[82] L. R. Merte, P. A. T. Olsson, M. Shipilin, J. Gustafson, F. Bertram, C. Zhang, H. Grönbeck, and E. Lundgren, Structure of two-dimensional Fe_3O_4, J. Chem. Phys. **152**, 114705 (2020).

[83] P. A. T. Olsson, L. R. Merte, and H. Grönbeck, Stability, magnetic order, and electronic properties of ultrathin Fe_3O_4 nanosheets, Phys. Rev. B **101**, 155426 (2020).

[84] M. Born, On the stability of crystal lattices. I, Math. Proc. Cambridge Philos. Soc. **36**, 160 (1940).

[85] F. Mouhat and F. X. Coudert, Necessary and sufficient elastic stability conditions in various crystal systems, Phys. Rev. B **90**, 224104 (2014).

[86] N. A. Spaldin, A beginners guide to the modern theory of polarization, J. Solid State Chem. **195**, 2 (2012).

[87] R. D. King-Smith and D. Vanderbilt, Theory of polarization of crystalline solids, Phys. Rev. B **47**, 1651 (1993).

[88] D. Vanderbilt, *Berry Phases in Electronic Structure Theory: Electric Polarization, Orbital Magnetization and Topological Insulators* (Cambridge University, New York, 2018).

[89] M. V. Berry, Quantal phase factors accompanying adiabatic changes, Proc. R. Soc. A **392**, 45 (1984).

[90] J. Zak, Berry's phase for energy bands in solids, Phys. Rev. Lett. **62**, 2747 (1989).

[91] P. Giannozzi, S. Baroni, N. Bonini, M. Calandra, R. Car, C. Cavazzoni, D. Ceresoli, G. L. Chiarotti, M. Cococcioni, I. Dabo, A. D. Corso, S. de Gironcoli, S. Fabris, G. Fratesi, R. Gebauer, U. Gerstmann, C. Gougoussis, A. Kokalj, M. Lazzeri, L. Martin-Samos *et al.*, QUANTUM ESPRESSO: A modular and open-source software project for quantum simulations of materials, J. Phys.: Condens. Matter **21**, 395502 (2009).

[92] P. Giannozzi, O. Andreussi, T. Brumme, O. Bunau, M. Buongiorno Nardelli, M. Calandra, R. Car, C. Cavazzoni, D. Ceresoli, M. Cococcioni, N. Colonna, I. Carnimeo, A. Dal Corso, S. de Gironcoli, P. Delugas, R. A. DiStasio, Jr., A. Feretti, A. Floris, G. Fratesi, G. Fugalio *et al.*, Advanced capabilities for materials modelling with QUANTUM ESPRESSO, J. Phys.: Condens. Matter **29**, 465901 (2017).

[93] I. Carnimeo, S. Baroni, and P. Giannozzi, Fast hybrid density-functional computations using plane-wave beasis sets, Electron. Struct. **1**, 015009 (2019).

[94] D. R. Hamann, Optimized norm-conserving Vanderbilt pseudopotentials, Phys. Rev. B **88**, 085117 (2013).

[95] M. Schlipf and F. Gygi, Optimization algorithm for the generation of ONCV pseudopotentials, Comput. Phys. Commun. **196**, 36 (2015).

[96] H. J. Monkhorst and J. D. Pack, Special points for Brillouin-zone integrations, Phys. Rev. B **13**, 5188 (1976).

[97] C. G. Broyden, The convergence of a class of double-rank minimization algorithms 1. General considerations, IMA J. Appl. Math. **6**, 76 (1970).

[98] R. Fletcher, A new approach to variable metric algorithms, Comput. J. **13**, 317 (1970).

[99] D. Goldfarb, A family of variable-metric methods derived by variational means, Math. Comput. **24**, 23 (1970).

[100] D. F. Shanno, Conditioning of quasi-newton methods for function minimization, Math. Comput. **24**, 647 (1970).

[101] K. Momma and F. Izumi, VESTA: A three-dimensional visualization system for electronic and structural analysis, J. Appl. Crystallogr. **41**, 653 (2008).

[102] A. Kokalj, XCrySDen–a new program for displaying crystalline structures and electron densities, J. Mol. Graphics Modell. **17**, 176 (1999).

[103] G. Avitabile, R. Napolitano, B. Pirozzi, K. D. Rouse, M. W. Thomas, and B. T. M. Willis, Low temperature crystal structure of polyethylene: Results from a neutron diffraction study and from potential energy calculations, J. Polym. Sci. Polym. Lett. Ed. **13**, 351 (1975).

[104] S. Kavesh and J. M. Schultz, Lamellar and interlamellar structure in melt-crystallized polyethylene. I. Degree of crystallinity, atomic positions, particle size, and lattice disorder of the first and second kinds, J. Polym. Sci. A-2: Polym. Phys. **8**, 243 (1970).

[105] P. W. Teare, The Crystal Structure of Orthorhombic Hexatriacontane, $C_{36}H_{74}$, Acta Crystallogr. **12**, 294 (1959).

[106] R. Hasegawa, Y. Takahashi, Y. Chatani, and H. Tadokoro, Crystal structures of three crystalline forms of Poly(vinylidene fluoride), Polym. J. **3**, 600 (1972).

[107] C. W. Bunn, The crystal structure of long-chain normal paraffin hydrocarbons. The "shape" of the <CH2 group, Trans. Faraday Soc. **35**, 482 (1939).

[108] M. S. Miao, M.-L. Zhang, V. E. Van Doren, C. Van Alsenoy, and J. L. Martins, Density functional calculations on the structure of crystalline polyethylene under high pressures, J. Chem. Phys. **115**, 11317 (2001).

[109] J. Kleis, B. I. Lundqvist, D. C. Langreth, and E. Schröder, Towards a working density-functional theory for polymers: First-principles determination of the polyethylene crystal structure, Phys. Rev. B **76**, 100201(R) (2007).

[110] D. Vanderbilt, Soft self-consistent pseudopotentials in a generalized eigenvalue formalism, Phys. Rev. B **41**, 7892 (1990).

[111] K. F. Garrity, J. W. Bennett, K. M. Rabe, and D. Vanderbilt, Pseudopotentials for high-throughput DFT calculations, Comput. Mater. Sci. **81**, 446 (2014).

[112] I.-C. Yeh, J. W. Andzelm, and G. C. Rutledge, Mechanical and structural characterization of semicrystalline polyethylene under tensile deformation by molecular dynamics simulations, Macromolecules **48**, 4228 (2015).

[113] I.-C. Yeh, J. L. Lenhart, G. C. Rutledge, and J. W. Andzelm, Molecular dynamics simulation of the effects of layer thickness and chain tilt on tensile deformation mechanisms of semicrystalline polyethylene, Macromolecules **50**, 1700 (2017).

[114] S. Lee and G. C. Rutledge, Plastic deformation of semicrystalline polyethylene by molecular simulation, Macromolecules **44**, 3096 (2011).

[115] J. M. Kim, R. Locker, and G. C. Rutledge, Plastic deformation of semicrystalline polyethylene under extension, compression, and shear using molecular dynamics simulation, Macromolecules **47**, 2515 (2014).

[116] M. Dewapriya and R. Miller, Molecular dynamics study of the penetration resistance of multilayer polymer/ceramic nanocomposites under supersonic projectile impacts, Extreme Mech. Lett. **44**, 101238 (2021).

[117] A. Apostoluk, C. Fiorini-Debuisschert, and J.-M. Nunzi, All optical poling in polymers and applications, in *Photoreactive*

Organic Thin Films, edited by Z. Sekkat and W. Knoll (Academic Press, San Diego, 2002), pp. 331–363.

[118] M. Smith and S. Kar-Narayan, Piezoelectric polymers: Theory, challenges and opportunities, Int. Mater. Rev. **67**, 65 (2022).

[119] Y. Roh, V. Varadan, and V. Varadan, Characterization of all the elastic, dielectric, and piezoelectric constants of uniaxially oriented poled PVDF films, IEEE Transactions on Ultrasonics, Ferroelectrics, and Frequency Control **49**, 836 (2002).

[120] A. S. Argon, *The Physics of Deformation and Fracture of Polymers* (Cambridge University, New York, 2013).

[121] P. J. Barham and A. Keller, The achievement of high-modulus polyethylene fibers and the modulus of polyethylene crystals, J. Polym. Sci. Polym. Lett. Ed. **17**, 591 (1979).

[122] L. Holliday and J. W. White, The stiffness of polymers in relation to their structure, Pure Appl. Chem. **26**, 545 (1971).

[123] R. F. Schaufele and T. Shimanouchi, Longitudinal acoustical vibrations of finite polymethylene chains, J. Chem. Phys. **47**, 3605 (1967).

[124] Y. Pei and X. C. Zeng, Elastic properties of poly(vinyldene fluoride) (PVDF) crystals: A density functional theory study, J. Appl. Phys. **109**, 093514 (2011).

[125] Y. Zhao, W. Yang, Y. Zhou, Y. Chen, X. Cao, Y. Yang, J. Xu, and Y. Jiang, Effect of crystalline phase on the dielectric and energy storage properties of poly(vinylidene fluoride), J. Mater. Sci.: Mater. Electron. **27**, 7280 (2016).

[126] D. V. Schroeder, *An Introduction to Thermal Physics* (Oxford University, New York, 2021).

[127] L. E. Reichl, *A Modern Course in Statistical Physics*, 4th ed. (Wiley, New York, 2016).

[128] O. H. Nielsen and R. M. Martin, Quantum mechanical theory of stress and force, Phys. Rev. B **32**, 3780 (1985).

[129] C. Ruberto, Y. Yourdshahyan, and B. I. Lundqvist, Stability of a flexible polar ionic crystal surface: Metastable alumina and one-dimensional surface metallicity, Phys. Rev. Lett. **88**, 226101 (2002).

[130] C. Ruberto, Y. Yourdshahyan, and B. I. Lundqvist, Surface properties of metastable alumina: A comparative study of κ- and α-Al_2O_3, Phys. Rev. B **67**, 195412 (2003).

[131] B. Razaznejad, C. Ruberto, P. Hyldgaard, and B. I. Lundqvist, Self-organized one-dimensional electron systems on a low-symmetry oxide surface, Phys. Rev. Lett. **90**, 236803 (2003).

[132] J. Rohrer, C. Ruberto, and P. Hyldgaard, *Ab initio* structure modelling of complex thin-film oxides: Thermodynamical stability of TiC/thin-film alumina, J. Phys.: Condens. Matter **22**, 015004 (2010).

[133] J. Rohrer and P. Hyldgaard, Understanding adhesion at as-deposited interfaces from *ab initio* thermodynamics of deposition growth: Thin-film alumina on titanium carbide, J. Phys.: Condens. Matter **22**, 472001 (2010).

[134] R. Sabatini, E. Kucukbenli, B. Kolb, T. Thonhauser, and S. de Ronkoli, Structural evolution of amino acid crystals under stress from a non-empirical density functional, J. Phys.: Condens. Matter **24**, 424209 (2012).